ISSN 1070-3284, Russian Journal of Coordination Chemistry, 2019, Vol. 45, No. 6, pp. 420–426. © Pleiades Publishing, Ltd., 2019.
Russian Text © The Author(s), 2019, published in Koordinatsionnaya Khimiya, 2019, Vol. 45, No. 6, pp. 359–365.

Computer Simulation of the Destruction of the Organic Lanthanide Complexes under Ionizing Radiation

S. V. Obolenskii[a, *], A. V. Kukinov[a, b], T. V. Balashova[b], A. N. Trufanov[c], M. N. Ivin[c], O. V. Kuznetsova[b], and M. N. Bochkarev[a, b, **]

[a] *Lobachevsky State University of Nizhny Novgorod, Nizhny Novgorod, Russia*
[b] *Razuvaev Institute of Organometallic Chemistry, Russian Academy of Sciences, Nizhny Novgorod, Russia*
[c] *Sedakov Research Institute of Measuring Systems, Nizhny Novgorod, Russia*
**e-mail: obolensk@rf.unn.ru*
***e-mail: mboch@iomc.ras.ru*

Received July 6, 2018; revised November 21, 2018; accepted December 3, 2018

Abstract—The calculation of defects in the structures of the Sc, La, Nd, Sm, Tb, and Yb complexes with substituted phenolate and naphtholate ligands formed under the action of neutrons with a mean energy of 2 MeV shows that the shifts of the target atoms depend on their masses and can achieve 1 μm for O, N, and S. A similar result is obtained for the calculation of the destruction of the $Eu(TTA)_3(DME)_2$ complex (HTTA is thenoyltrifluoroacetone). However, the treatment of the samples with the *n*,γ radiation does not result in destruction. Possible reasons for the found divergence between the calculated and experimental data are discussed.

Keywords: scandium, lanthanides, neutrons, irradiation, destruction, simulation, luminescence
DOI: 10.1134/S1070328419050014

INTRODUCTION

Semiconductors find wide use in science and technology, including devices and instruments that can be prone to radiation when applied in space vehicles, nuclear power plants of various design, and/or defense technology. The common feature of these materials is their composition: all of them are inorganic substances. Organic compounds, in particular, the organic complexes of rare-earth metals, have a number of advantages over the inorganic analogs, which make them promising for applying in many special areas [1]. Therefore, there is a problem of determining the level of radiation resistance of organic semiconductors to γ-quanta and neutrons.

In order to fill the aforementioned gap, we calculated the cross sections and simulated the interactions of neutrons of the fission spectrum of uranium nuclei with all types of atoms that are met in the phenolate, naphtholate, and similar lanthanide complexes using the SRIM-2003 program. The compounds used for simulation were synthesized and characterized previously [1–3] and differ in the type of metals, elemental composition, and ligand size. The organic compound, *N*,*N*'-diphenyl-*N*,*N*'-bis(3-methylphenyl)-1,1'-biphenyl-4,4'-diamine (TPD), applied as a hole-transporting material in organic light diodes was modeled for comparison. The IR and photoluminescence spectra of the studied compounds were compared in order to determine a qualitative change in the compounds after the treatment.

EXPERIMENTAL

Dimethoxyethane (DME) was dehydrated with sodium benzophenone ketyl using a standard procedure and was taken in vacuo prior to use. The europium silylamide complex $Eu[N(SiMe_3)_2]_3$ was synthesized using a known procedure [4]. Commercial (Aldrich) thenoyltrifluoroacetone (HTTA) was used as received. The compounds chosen for simulation, $[Ln(OON)_3]_2$ (OON is 2-(2-benzoxazol-2-yl)phenolate), $[Ln(SON)_3]_2$ (SON is 2-(2-benzothiazol-2-yl)phenolate) [2], $[Ln(NpOON)_3]_2$ (NpOON is 3-(2-benzoxazol-2-yl)-2-naphtholate), and $[Ln(NpSON)_3]_2$ (NpSON is 3-(2-benzothiazol-2-yl)-2-naphtholate [3], were synthesized using the previously developed procedures.

Synthesis of $Eu(TTA)_3(DME)_2$ was carried out using the standard Schlenk technique under the conditions excluding contact with air oxygen and moisture. A solution of HTTA (70 mg, 0.315 mmol) in DME (10 mL) was added to a solution of $Eu[N(SiMe_3)_2]_3$ (67 mg, 0.106 mmol) in DME

(5 mL). The reaction mixture was stirred for 30 min at room temperature. The color of the solution changed from red to light yellow, and DME and other volatile reaction products were removed by condensation in vacuo. The solid residue was washed with hexane and dried in vacuo. The yield was 81 mg (77%).

For $C_{32}H_{35}F_9O_{10}S_3Eu$				
Anal. calcd., %	C, 38.48	H, 3.53	S, 9.63	Eu, 15.22
Found, %	C, 38.54	H, 3.61	S, 9.68	Eu, 15.07

IR (ν, cm^{-1}): 3104 w, 1627 m, 1601 m, 1580 m, 1537 m, 1509 m, 1413 m, 1352 m, 1307 m, 1252 m, 1232 m, 1182 m, 1139 m, 1054 m, 933 m, 862 m, 792 m, 769 w, 750 w, 736 w, 711 m, 684 s, 641 s, 606 w, 581 s, 561 w, 519 w, 498 m.

The IR spectra of the samples as suspensions in Nujol were recorded between KBr windows on an FSM 1201 FTIR spectrometer (OOO Monitoring, Russia) in a range of 4000–400 cm^{-1}. An LS 55 luminescence spectrometer (PerkinElmer, USA) was used for recording the emission spectra in the range from 200 to 800 nm. Solid samples and solutions of the compounds in acetonitrile with a concentration of 0.3 mmol/L were used. A nuclear reactor served as an *n*,γ-radiation source. The samples were placed in sealed glass ampules.

Mathematical model. The cross sections of the interaction of neutrons with atoms of the complexes were calculated for a mean neutron energy of 2 MeV, and additional calculations were performed for an energy of 100 keV and 10 MeV. The neutron radiation energy was varied during calculations, and the trial calculation of the action of γ-quanta was performed. The calculation results were analyzed on the basis of the data of statistical averaging of the distribution of radiation defects, ionization, and heating (phonons). The defect formation processes in the studied materials were compared for the light and heavy atoms composing the materials. The obtained results were compared to the classical semiconductor materials (silicon and gallium arsenide).

The calculation was performed by the Monte Carlo method using the SRIM-2003 software package [5]. The trajectory of each recoil atom gained an energy upon a neutron impact started from the introduction of its position, direction of motion, and energy. In the free path length of the recoil atoms, their energy decreased by the value of electron losses to the ionization of the material. After collision, the energy decreased by the value of the so-called nuclear (or elastic) energy losses, i.e., by the energy transmitted to the target atom on collision. The trajectory of the recoil atom was considered broken if its energy decreased to the value lower than the preliminarily specified one.

The energy transmitted by neutrons to the recoil atoms and responsible for radiation violations was calculated by the following equation [5]:

$$T_A = \frac{4M_nM_A}{(M_n + M_A)^2} T_n \sin^2(\theta/2) = \frac{4A}{(1+A)^2} T_n, \quad (1)$$

where M_n and M_A are the masses of the neutron and atom, respectively; T_n is the kinetic energy of the bombarding neutron; θ is the recoil angle between the direction of neutron motion before and after collision; and A is the atomic mass.

The scattering angle in the system of the center of gravity was determined as follows [5]:

$$\cos\theta = \frac{P + \rho + \delta}{\rho + r_0}. \quad (2)$$

The target atoms were chosen using random numbers under the assumption that the probability of collision with the atom of each type was proportional to its stoichiometric coefficient determined by the empirical formula. The distinction between the light and heavy atoms in the target was the value of the interaction potential.

Electron losses were determined as the product of the stopping function by the free path length of the recoil atom according to the model of nonlocal energy losses [6]. The Bragg rule stating that the contribution of each type of target atoms to the stopping ability is proportional to the atomic fraction of these atoms was used.

The calculation procedure was reduced to the determination of the concentration of radiation defects for all types of recoil atoms in the studied materials in the ratio corresponding to the empirical formulas of the substances. The defect distribution in the space was also examined, and the ionization and local warming of the studied materials were compared.

RESULTS AND DISCUSSION

The compounds used in the calculations and their empirical formulas and densities are presented in Table 1.

The molecular structures have earlier been determined for the most part of the complexes by X-ray diffraction analysis [2, 3]. The schematically presented molecules of the compounds used in the simulation of radiation destruction differ in the general structure, metal, elemental composition, and ligand volume.

Table 1. Compounds used for the simulation

Compound	Empirical formula	Density, g/cm^3
$Sc(NON)_3$	$C_{47}H_{43}N_6O_5Sc$	1.391
$Sc(OON)_3$	$C_{39}H_{24}N_3O_6Sc$	1.473
$Sc(NpOON^{Me})_3$	$C_{54}H_{46}N_3O_{7.50}Sc$	1.283
$[La(OON)_3]_2$	$C_{78}H_{48}La_2N_6O_{12}$	1.681
$[Nd(OON)_3]_2$	$C_{78}H_{48}N_6Nd_2O_{12}$	1.683
$[Nd(NpOON)_3]_2$	$C_{102}H_{60}N_6Nd_2O_{12}$	1.622
$[Sm(OON)_3]_2$	$C_{78}H_{48}N_6O_{12}Sm_2$	1.658
$[Ce(OON)_3]_2$	$C_{78}H_{48}Ce_2N_6O_{12}$	1.656
$[Yb(OON)_3]_2$	$C_{78}H_{48}N_6O_{12}Yb_2$	1.660
$[Sm(SON)_3]_2$	$C_{78}H_{48}N_6O_6S_6Sm_2$	1.752
$[Sm(NpOON)_3]_2$	$C_{102}H_{60}N_6O_{12}Sm_2$	1.622
$Eu(TTA)_3(DME)_2$	$C_{32}H_{25}EuO_{10}S_3$	1.72
TPD	$C_{38}H_{32}N_2$	1.16

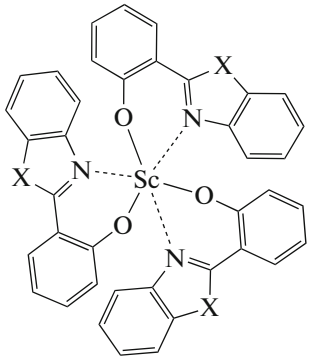

X = O (OON); S (SON)

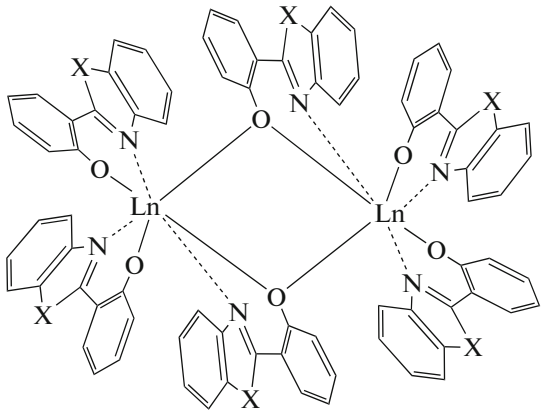

X = O (OON); S (SON)

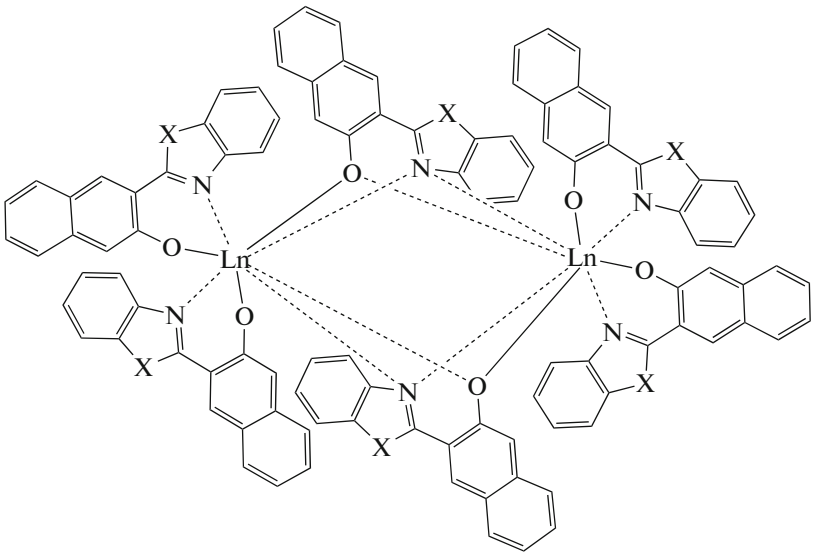

X = O (NpOON); S (NpSON)

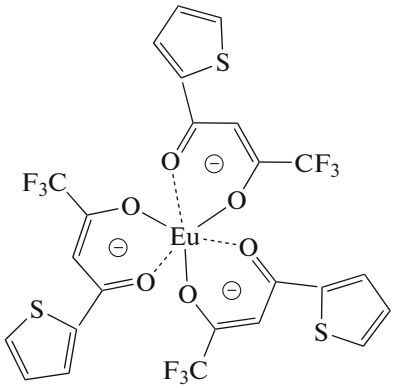

$Eu(TTA)_3$

Table 2. Neutron scattering cross sections and the mean energy transmitted to the recoil atoms (for neutrons with the energy 2 MeV)

Element	Atomic mass	Scattering cross section, barn	Energy transmitted to recoil atom, keV
H	1	13	2000
C	12	2	568
N	14	2	500
O	16	2	443
Sc	45	4	170
La	139	5	57
Ce	140	5	56
Nd	142	5	54
Sm	150	5.1	53
Eu	152	5.1	52
Yb	173	5.3	46

In the studied molecules, the total energy of chemical bonds of an individual atom with adjacent atoms did not exceed 40 eV, which is by three orders of magnitude lower than the energy of fast neutrons and, hence, cannot affect the radiation resistance of the compounds. On the contrary, the energies of slow neutrons and secondary recoil atoms are comparable with the energies of chemical bonds, which can favor the enhancement of the resistance of the material.

According to the Breit–Wigner theory, the cross section of neutron elastic scattering on atoms is the sum of three terms describing the elastic scattering cross section $4\pi a^2$ (where a is the radius of the atomic nucleus), resonance scattering, and their interference.

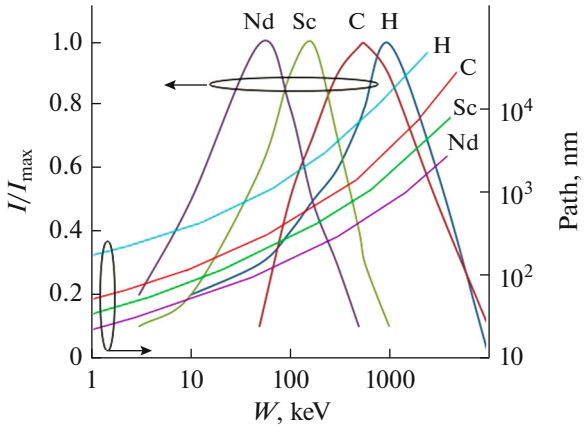

Fig. 1. Energy spectra and the paths of the primary Nd, Sc, C, and H atoms gained an energy due to the interaction with neutrons of the fission spectrum (the paths are presented for $Sc(NON)_3$, and the paths for other studied materials differ by 15–30%).

Since the resonance interaction is complicated, the dependence of the cross section on the neutron energy contains several narrow peaks. The widths of these peaks are small compared to the spectrum of the neutron radiation of a nuclear reactor. The averaged dependence can deviate to both lower and higher values and, hence, averaged spectra can be used when considering the integrated interaction for which the narrow peaks would compensate each other. The overall result can be presented as a sum of the elastic and nonelastic scattering and the effect of neutron absorption related to nuclear reactions. A distinctive feature of the reactions with the neutron energies from 10 keV to 2–3 MeV is that the processes with elastic scattering are the most probable, while other processes are either poorly probable or forbidden by energy. The average cross sections of neutrons scattered on the atomic nuclei used in the work are presented in Table 2.

The spectra of the Nd, Sc, C, and H atoms gained an energy due to the interaction with neutrons of the fission spectrum are presented in Fig. 1 along with the paths of the Sc, C, and H recoil atoms gained an energy due to the interaction with neutrons in $Sc(NON)_3$ and Nd in $[Nd(OON)_3]_2$. A comparison of the path lengths of other atoms in other studied materials shows that their difference is not higher than 10–20%. This is explained by similar chemical compositions and comparable densities of the materials.

The external view of the shift cascades in $[Nd(OON)_3]_2$ is presented in Fig. 2. Each point of the image corresponds to the shifted atom. It was assumed that a neutron transmitted the energy to the atoms at the corresponding starting point in the vertical axis and their primary impulse was directed to the right. The primary recoil atom moves "from left to right"

and forms a chain of the shifted atoms along the trajectory. The secondary recoil atoms gained significant energies from the primary atoms form subcascades of the shifted atoms. The shift cascades differ substantially for the primary atoms of various masses: the heavy atoms form dense aggregates (clusters) of defects, whereas the light atoms form strongly elongated aggregates with an increased concentration of defects at the end of the path of the primary recoil atom. The initial energy of the recoil atoms substantially affects the characteristic sizes of the defect clusters (see the path lengths in Fig. 1). The cross sections of the interaction of the primary atoms with the secondary atoms also depend substantially on the ratio of masses of the incident atom and target atom, and the number of primary atoms with various energies is determined by their energy spectra (Fig. 1). Therefore, the calculation of the defect concentration under the neutron irradiation of the studied materials is a nontrivial task and was solved by the Monte Carlo method described above.

The ratio of the number of radiation defects per 1000 primary atoms shifted by neutrons is presented in Table 3. A comparison of the data shows that in the materials with Sc the main defects will be generated by the primary carbon atoms, while in $Nd_2(OON)_6$ neodymium is the major atom forming radiation defects. Taking into account the fact that the cross section of the interaction of neodymium with neutrons is higher than that of scandium, we may conclude that the materials with scandium are more resistant to radiation. The radiation resistance increases by ~25% in the series of materials $Sc(OON)_3$, $Sc(NON)_3$, and $Sc(NpOON^{Me})_3$. The resistances of the $[La(OON)_3]_2$, $[Nd(OON)_3]_2$, and $[Yb(OON)_3]_2$ materials differ insignificantly.

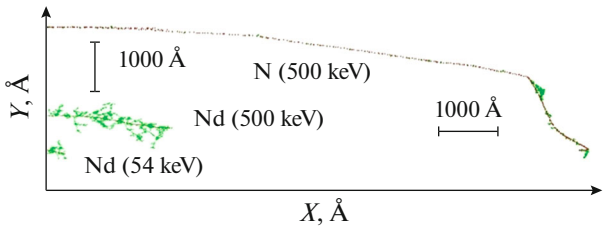

Fig. 2. Comparison of the cascades of the recoil atoms formed by the primary Nd (54 and 500 keV) and N (500 keV) atoms in $[Nd(OON)_3]_2$.

According to the calculations (Tables 2, 3; Figs. 2, 3), all compounds studied undergo deep transformations upon the action of fission neutrons. This should drastically change their physicochemical properties similarly to the changes observed in the inorganic semiconductors [7–9].

The chosen $Eu(TTA)_3(DME)_2$ and $[La(NpSON)_3]_2$ complexes were subjected to the pulse treatment with fission neutrons and γ-photons (3 ms, absorbed dose 130 krad, and fluence 3.6×10^{13} J/cm^2) to evaluate the adequacy of modeling the real processes that occur in the organometallic materials under the high-energy ionizing irradiation. The irradiation did not result in a change in the exterior, color, and IR and photoluminescence spectra of the samples (Fig. 3). It should be mentioned that the Eu^{3+} ion (*f*–*f* transition $^5D_0$–$^7F_2$) is the emission center in the europium complex, whereas the luminescence band of the ligands is detected in the spectrum of the lanthanum complex. Interestingly, the X-ray irradiation of the $CaAlO_4$:Eu inorganic material induces the reduction of Eu^{3+} to Eu^{2+}, which is distinctly observed in the photoemission spectrum [10].

Table 3. Ratio of the number of radiation defects per 1000 primary atoms shifted by neutrons (for the energy of the recoil atom indicated in Table 2)

Primary target atom	Complex					
	$Sc(OON)_3$	$Sc(NON)_3$	$Sc(NpOON^{Me})_3$	$[La(OON)_3]_2$	$[Nd(OON)_3]_2$	$[Yb(OON)_3]_2$
H	63	76	66	71	72	74
C	251	205	193	281	287	283
N	18	25	9	21	21	21
O	34	19	22	38	39	38
Sc	105	70	51			
La				816		
Nd					828	
Yb						892

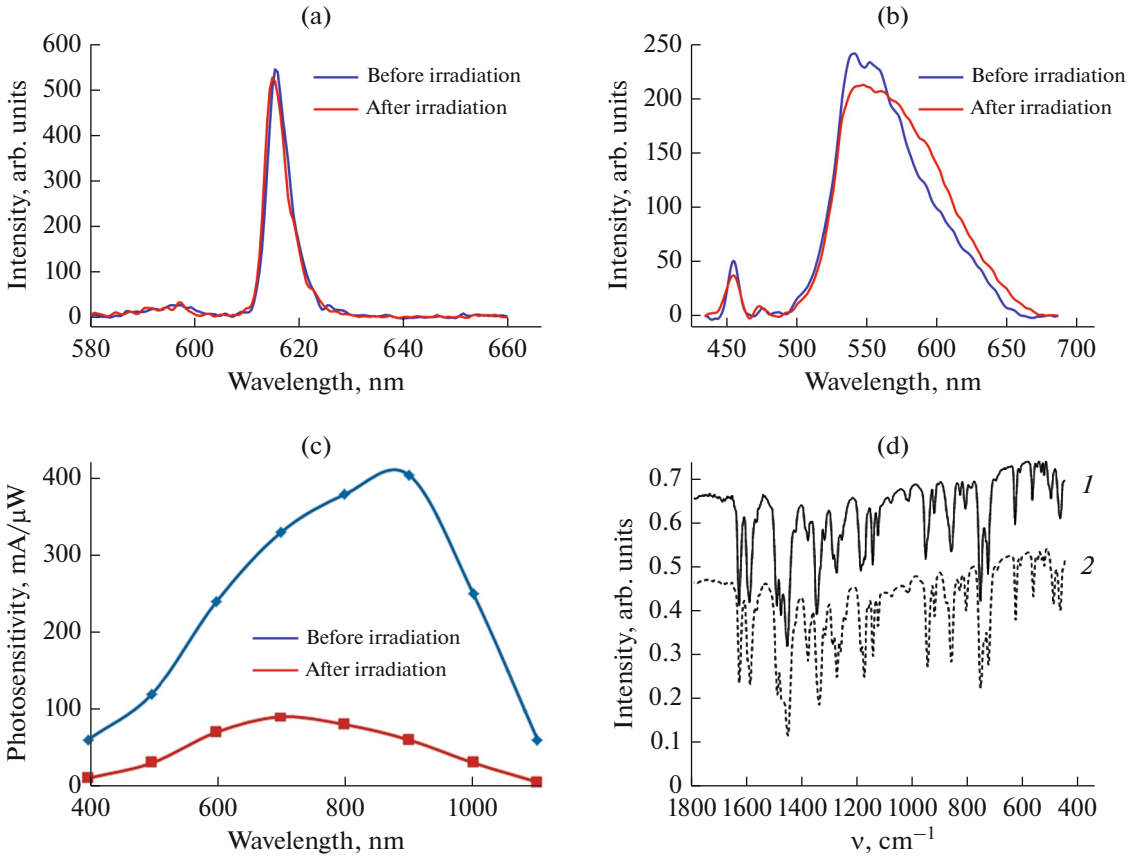

Fig. 3. Photoluminescence spectra of the (a) $Eu(TTA)_3(DME)_2$ complex in a THF solution at λ_{exc} = 395 nm and (b) solid $[La(NpSON)_3]_2$ complex at λ_{exc} = 390 nm; (c) the spectral photosensitivity of silicon and (d) the IR spectra of the $[La(NpSON)_3]_2$ complex (*1*) before and (*2*) after irradiation. The spectra before and after γ-neutron irradiation with a fluence of 10^{14} J cm^{-2} for the organic semiconductors (a, b) and 10^{13} J cm^{-2} for the silicon *p*–*n* transition.

The found divergence between the calculated and experimental data is explained, most likely, by a low density of the organic semiconductors compared to the inorganic analogs and by another luminescence mechanism.

An analysis of the nonuniform energy release and radiation defects in the bulk of diphenyl-*N*,*N*'-bis(3-methylphenyl)-1,1'-biphenyl-4,4'-diamine and organic complexes of neodymium, samarium, lanthanum, europium, ytterbium, and scandium upon the insertion of hydrogen, carbon, nitrogen and metal atoms during neutron, electron, and γ-irradiation shows that the organic semiconductors are characterized by significantly more rarefied clusters of radiation defects than the inorganic semiconductor materials, which makes it possible to recommend them as promising materials for radiation-resistant electronics.

It is found by the simulation of fast electron scattering in the metal complexes of neodymium, samarium, scandium, and TPD that the concentration of defects formed in the studied materials is by 3–4 orders of magnitude lower than that observed for neutron irradiation. In addition, no defect clusters are observed in the materials, and only point defects and their complexes are formed. These data, calculation results of the destruction of the complexes under neutron irradiation, and results of the treatment of the samples with *n*,γ radiation indicate that the studied materials are highly resistant to radiation and, hence, can be recommended as a basis for manufacturing radiation-resistant energy converters, first of all, autonomous current sources characterized by the prolonged operation and based on β-radiating isotopes (β-cells [11–13]).

FUNDING

This work was supported by the Russian Science Foundation (project no. 18-03-00066). The synthesis of the compounds was supported by the Russian Foundation for Basic Research (project no. 18-03-00241).

REFERENCES

1. *Lanthanide Luminescence: Photophysical, Analytical and Biological Aspects*, Pekka, H., and Harri, H., Eds., Springer Ser. Fluoresc., 2011, vol. 7.

2. Balashova, T.V., Pushkarev, A.P., Ilichev, V.A., et al., *Polyhedron*, 2013, vol. 50, p. 112.

3. Burin, M.E., Kuzyaev, D.M., Lopatin, M.A., et al., *Synth. Met.*, 2013, vol. 164, p. 55.

4. Bradley, D.C., Ghotra, J.S., and Hart, F.A., *J. Chem. Soc., Dalton Trans.*, 1973, no. 10, p. 1021.

5. Biersak, J.P., *Nucl. Instruments Methods Phys. Res.*, 1987, no. 1, p. 2136.

6. Grigor'ev, I.S. and Meilikhov, E.Z. *Fizicheskie velichiny* (Physical Quantities), Moscow: Energoatomizdat, 1991.

7. Lei, Y., Yang, Y., Liu, Y., et al., *Appl. Radiation Isotopes*, 2014, vol. 90, p. 165.

8. Okuno, Y., Okuda, S., Akiyoshi, M., et al., *J. Appl. Phys.*, 2017, vol. 122, p. 114901.

9. Kawakita, S., Imaizumi1, M., Ishizuka, S., et al., *Phys. Status Solidi. C*, 2017, p. 1600168.

10. Gomes, M.A., Carvalho, J.C., Andrade, A.B., et al., *Opt. Mater.*, 2018, vol. 75, p. 122.

11. Sychov, M., Kavetsky, A., Yakubova, G., et al., *Appl. Radiat. Isot.*, 2008, vol. 66, p. 173.

12. Russoa, J., Litza, M., Ray, II, W., et al., *Appl. Radiation Isotopes*, 2017, vol. 130, p. 66.

13. Zhanga, Z.-R., Liu, Y.-P., Tanga, X.-B., et al., *Nucl. Instruments Methods Phys. Res*. B, 2018, vol. 415, p. 9.

Translated by E. Yablonskaya